PHASE UNWRAPPING

LESLIE YING
University of Wisconsin-Milwaukee
Milwaukee, WI

1. INTRODUCTION

It is well known that the phase of a complex function is uniquely defined only in the principal value range. Recovering the original phase values from the principal values is a classic signal processing problem often known as phase unwrapping. This problem originates in a variety of applications, such as terrain elevation estimation in synthetic aperture radar (SAR) (1), field mapping in magnetic resonance imaging (MRI) (2), wavefront distortion measurement in adaptive optics (3), and accurate profiling of mechanical parts by x-ray. As an example, let us look at Thomas Young's interference experiment shown in Fig. 1a, in which a single source generates two beams through two slits. Because the beams are correlated and spatially coherent, the view screen on the right displays the intensity of the interfering light waves and shows a series of bright lines and dark bands as in Fig. 1b. The intensity at a certain point of the screen depends on the phase ϕ of the interference wave, which is proportional to the path difference $r_1 - r_2$ between the two beams traveling from the slits to the point. Constructive interference occurs, producing bright bands if

$$\phi = 2\pi \frac{r_1 - r_2}{\lambda} = 2k\pi, \tag{1}$$

where k is an integer and λ is the wavelength, whereas destructive interference occurs, producing dark bands if

$$\phi = 2\pi \frac{r_1 - r_2}{\lambda} = (2k+1)\pi. \tag{2}$$

Thus, the interference pattern can be used directly to measure the path difference $r_1 - r_2$ at any point of the screen. However, because of the periodic characteristics of the interfering waves, the phase at a certain point is uniquely defined only in the principal value range of $(-\pi, \pi]$. For example, given that the intensity at P in Fig. 1 is at a maximum, it can be concluded that the path difference is an integer multiple of the wavelength, but the integer value cannot be determined without additional information. Finding the hidden integer is a one-dimensional (1-D) phase unwrapping problem. If the slits in Fig. 1a are changed to pinholes, the interference pattern and the phase unwrapping problem will become two-dimensional (2-D). Figures 2a and b show the corresponding 2-D interference pattern and the image of wrapped phase.

1.1. Definitions and Properties

Formally, the phase unwrapping problem can be defined as given the wrapped phase $\psi \in (-\pi, \pi]$, find the "true"

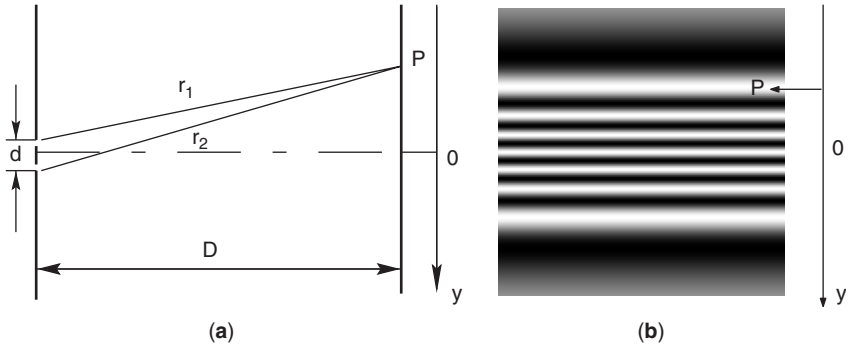

Figure 1. (a) The geometry of the Young's interference experiment and (b) the interference pattern.

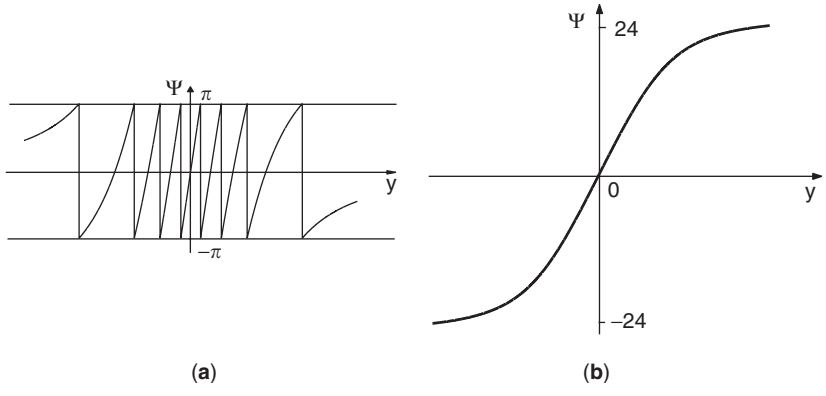

Figure 2. The (a) intensity and the (b) wrapped phase of a 2-D Young's interference pattern.

phase ϕ, which is related to ψ by

$$\psi = \mathcal{W}(\phi) = \phi - 2\pi\left\langle \frac{\phi}{2\pi} \right\rangle, \tag{3}$$

where $\mathcal{W}$ is the wrapping operator and $\langle \bullet \rangle$ rounds its argument to the closest integer. Because the wrapping operation is surjective but not injective, phase unwrapping is mathematically ill posed in general. However, in practice, the true phase value at a certain point is not independent of its spatial or temporal context. The latter can provide additional information to make unwrapping possible, which is the crux of phase unwrapping. For example, in Young's interference experiment described in the previous section, by imposing that $r_1 - r_2$ changes continuously with y, the integer multiple of 2π to be added to (for positive y) or subtracted from (for negative y) the wrapped phase can be determined by counting the number of bright bands between the reference center and the point of interest, and thus the phase unwrapping problem is solved!

1.1.1. One-Dimensional Phase Unwrapping. One-dimensional phase unwrapping can be solved easily if phase continuity is assumed. In 1982, Itoh analyzed the 1-D phase unwrapping problem and showed that the wrapped phase gradient modulo 2π are the same as the corresponding true phase gradient if the latter is less than π in radian everywhere (4). This fact implies that given the above condition, the unwrapped phase can be obtained by integrating the modulo wrapped phase gradient. This result is summarized in Lemma 1.1 with respect to sampled phase values.

Lemma 1.1. *Let*

$$\Delta\phi_n = \phi_n - \phi_{n-1}, \quad \Delta\psi_n = \psi_n - \psi_{n-1}, \tag{4}$$

where ϕ_n and ψ_n represent the true and wrapped phase value, respectively. If the smoothness condition

$$|\Delta\phi_n| \leq \pi \tag{5}$$

is satisfied, then

$$\Delta\phi_n = \mathcal{W}(\Delta\psi_n). \tag{6}$$

The above property provides a straightforward way to unwrap the phase-by-phase integration if Equation 5 is satisfied. Figure 3b shows the unwrapped results of Fig. 3a in the Young's experiments based on Lemma 1.1. However, undersampling and noise could violate the smoothness condition and result in unwrapping errors. Figure 4 demonstrates how these two factors affect the unwrapping results. In Fig. 4a, the sampling rate is so low that Lemma 1.1 fails to give the correct phase signal. Figure 4b shows the unwrapping results with two different signal-to-noise ratios (SNRs), which are defined as the ratio between the signal power to the noise power of the complex signal. It demonstrates that the SNR needs to be sufficiently high to unwrap the phase successfully.

1.1.2. Two-Dimensional Phase Unwrapping. We represent 2-D phase values at pixel (m, n) by $\phi_{m,n}$. Similarly to Lemma 1.1, we have the following result for 2-D phase functions.

Lemma 1.2. *Let*

$$\begin{aligned} &\Delta_x\phi_{m,n} = \phi_{m,n} - \phi_{m-1,n}, \quad \Delta_y\phi_{m,n} = \phi_{m,n} - \phi_{m,n-1}, \\ &\Delta_x\psi_{m,n} = \psi_{m,n} - \psi_{m-1,n}, \quad \Delta_y\psi_{m,n} = \psi_{m,n} - \psi_{m,n-1}. \end{aligned} \tag{7}$$

If the following inequalities hold

$$|\Delta_x\phi_{m,n}| \leq \pi \text{ and } |\Delta_y\phi_{m,n}| \leq \pi, \tag{8}$$

then

$$\begin{aligned} \Delta_x\phi_{m,n} &= \mathcal{W}(\Delta_x\psi_{m,n}), \\ \Delta_y\phi_{m,n} &= \mathcal{W}(\Delta_y\psi_{m,n}). \end{aligned} \tag{9}$$

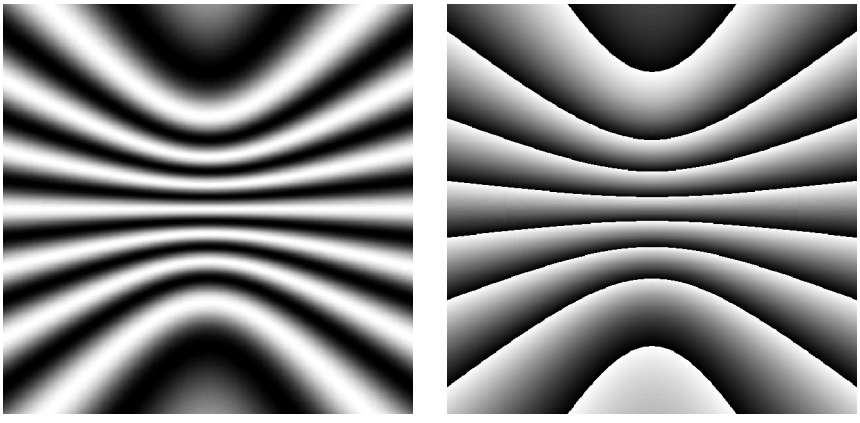

(a) (b)

Figure 3. The (a) wrapped and (b) unwrapped phase of a 1-D interference wave of the Young's experiment. Note that (b) exactly recovers the desired true phase.

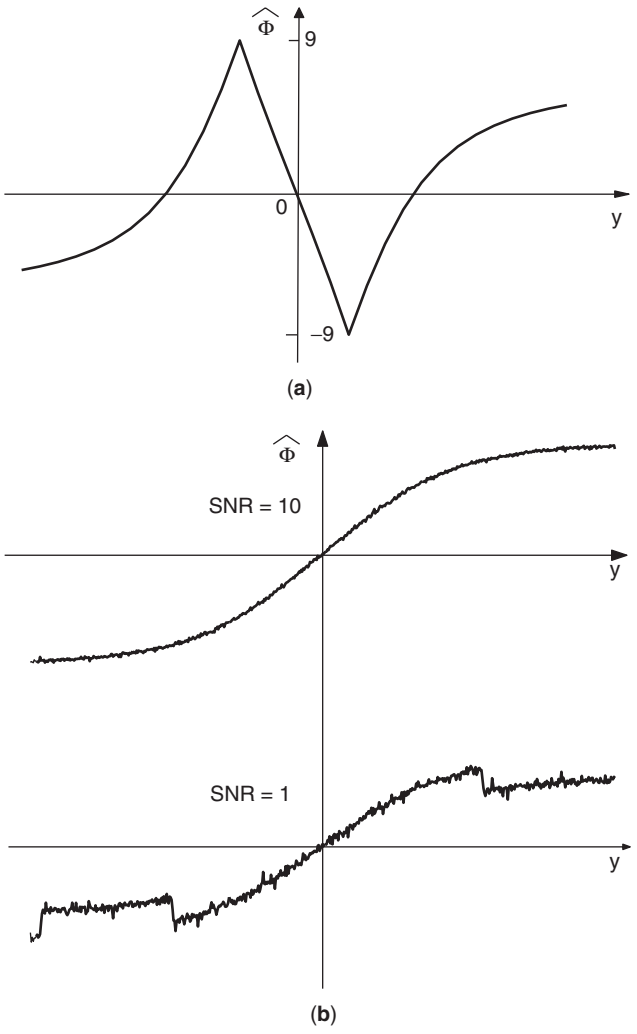

Figure 4. If the wrapped phase of Fig. 2 is undersampled, the resulting (a) unwrapped phase is incorrect. If the wrapped phase is noisy, it can be unwrapped correctly if the SNR is sufficiently high as shown on the top of (b), but it fails when SNR is low as shown at the bottom of (b).

The above result suggests that 2-D phase unwrapping can also be done by phase integration provided that the condition in Equation 8 is met. When the condition is violated, as is often the case in practice, the integration results will depend not only on the beginning and end points, but also on the chosen path of the line integral (5), which is illustrated in Fig. 5a, where phase values are shown in a gray scale ranging from $-\pi$ (black) to π (white). Visual inspection of the fringes shows that the unwrapped phase of the central pixel is the same as the wrapped one if the line integral follows the path of the solid line. However, if the line integral is along the dashed line, the unwrapped phase of the same pixel is the wrapped plus 2π. This inconsistency is known as the path-dependent problem in 2-D phase unwrapping.

Lemma 1.3 (6) lists several ways to test whether the integration of the phase gradients is path-independent.

Lemma 1.3. *Any of the following equivalent conditions must be satisfied to ensure that the line integral of the field represented by* $\mathcal{W}(\Delta\psi^x_{m,n})\vec{x} + \mathcal{W}(\Delta\psi^y_{m,n})\vec{y}$ *is path-independent, where* $\vec{x}$ *and* $\vec{y}$ *are the unit vectors in the x and y directions.*

- *A single-valued scalar function* $f_{m,n}$ *exists such that*

$$\mathcal{W}(\Delta_x\psi_{m,n})\vec{x} + \mathcal{W}(\Delta_y\psi_{m,n})\vec{y} = \Delta_x f_{m,n}\vec{x} + \Delta_y f_{m,n}\vec{y}.$$

- $\sum_C[\mathcal{W}(\Delta_x\psi_{m,n}) + \mathcal{W}(\Delta_y\psi_{m,n})] = 0$, *where* C *denotes any closed path.*
- $\Delta_y\mathcal{W}(\Delta_x\psi) \equiv \Delta_x\mathcal{W}(\Delta_y\psi)$.

In practice, the above conditions are seldom satisfied, and therefore, Lemma 1.2 cannot be used directly for phase unwrapping.

Accordingly, if unwrapping is path-dependent, $\sum_C[\mathcal{W}(\Delta_x\psi_{m,n}) + \mathcal{W}(\Delta_y\psi_{m,n})]$ is not always zero. The nonzero value is known as the *residue* (7). It can be caused by noise, spatial undersampling, or discontinuity in the original phase. A simple way to detect residues is to sum around every smallest possible closed path (say, a 2×2-sample path) in the entire phase image (8). The residues can be either positive or negative 2π. Figure 5b shows an

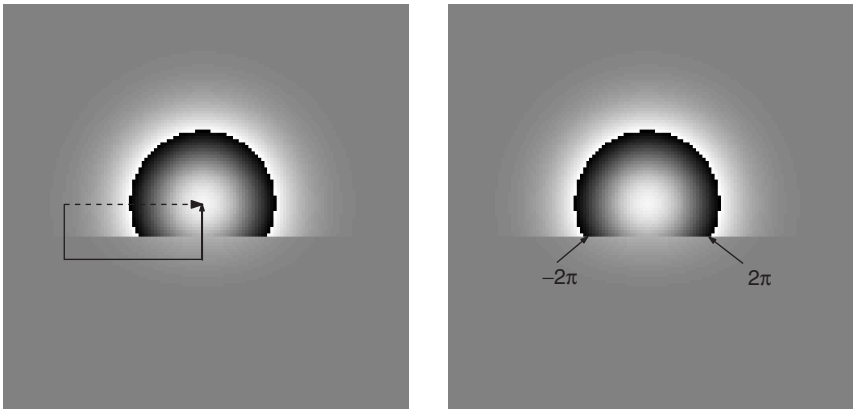

Figure 5. To illustration of the (a) path-dependent problem shows a wrapped phase image where the values are shown in a gray scale ranging from $-\pi$ (black) to π (white). The dashed path and the solid path have the same beginning and ending points, but they can result in different unwrapping results: The unwrapped phase of the central pixel keeps the same if unwrapping follows the solid path, but it adds 2π if unwrapping is along the dashed line. The path-dependent problem is from the existence of two residues with opposite polarities at the locations annoted in (b).

exemplary pair of residues with opposite polarities. Knowledge of the locations and the polarities of the residues can help avoid the path-dependent problem by choosing the integration path properly. Therefore, although 2-D phase unwrapping is more challenging than 1-D, it has more information to reduce noise sensitivity. For example, in the 1-D case, a phase unwrapping error at a single point will propagate to the rest of the unwrapped phase signal along the integration path, whereas the error could be avoided in 2-D because of the existence of multiple integration paths. By the same token, higher dimensional phase unwrapping can be even more robust to noise with the increased dimensionality. Recent development in three-dimensional (3-D) and N-D phase unwrapping has revealed these encouraging opportunities (9–11).

1.1.3. Characteristics of Phase Noise. The statistical properties of phase noise depend on several factors. Supposing additive Gaussian noise exists with zero mean and variance σ in both the real and the imaginary part of a complex image, the corresponding phase noise θ of the complex image is also additive and obeys the following probability distribution (12):

$$p(\theta) = \frac{\exp(-V_0^2/2\sigma^2)}{4\pi^2} + \frac{V_0 \cos\theta}{(2\pi)^{3/2}\sigma} \times \exp\left(-\frac{V_0^2 \sin^2\theta}{2\sigma^2}\right) \mathbf{Q}\left(\frac{V_0 \cos\theta}{\sigma}\right), \tag{10}$$

where V_0 are the magnitude of the clean image and $\mathbf{Q}(a) = \frac{1}{\sqrt{2\pi}} \int_{-\infty}^{a} e^{-x^2/2}\, dx$. Note that the density function depends on the SNR, denoted by $(V_0^2/2\sigma^2)$ in decibels. Figure 6 shows some examples of how SNR affects the shape of the density function.

Phase noise is an important source of residues. The total number of residues is statistically one third of the number of pixels in a totally random phase map (9). These residues usually need to have an equal number of positive and negative signs for unambiguous phase unwrapping.

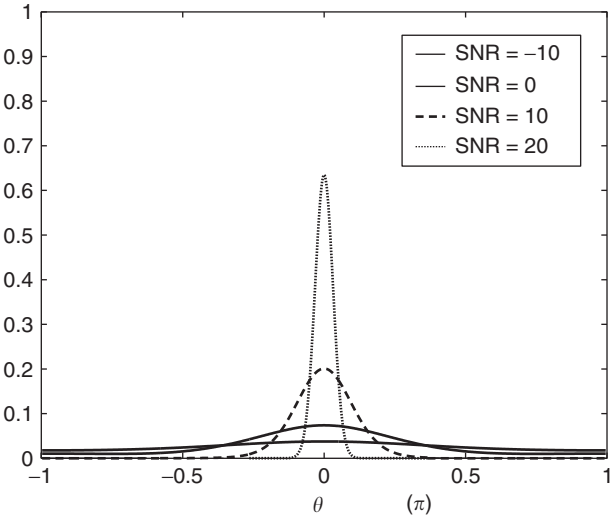

Figure 6. Distribution of phase noise at different SNRs.

1.1.4. Congruent Test. The true phase is usually unobtainable in practice. As a result, a congruent test is often used to validate the results of a phase unwrapping algorithm. This test is motivated by the fact that $\mathcal{W}(\Phi - \Psi) = 0$ for the true phase and replaces Φ with the estimated unwrapped phase $\hat{\Phi}$ to check if the relation still holds.

2. PHASE UNWRAPPING ALGORITHMS

2.1. Literature Review

Much work has been done on 2-D phase unwrapping, which has resulted in many practical algorithms. For convenience, we may group these methods into three main categories: minimum-norm, branch cuts, and network flow methods, although several techniques that do not fit naturally into the above three categories [e.g., the techniques using "Cellular automata" (5), temporal phase unwrapping (13), and 3-D (9,10) or N-D phase unwrapping (11)].

The minimum-norm methods formulate the phase unwrapping problem in a generalized minimum-norm sense. They seek a phase function whose unwrapped phase gradients are both path-independent and as close as possible to the measured wrapped phase gradients. If the L_2 norm is used to measure the fitting error (as is done in the least-squares methods), the optimization problem has an analytical solution, which is given by the discrete form of Poisson's equation with Neumann boundary conditions. The unweighted least-squares method can be efficiently implemented using the fast Fourier transform (FFT) (14), discrete cosine transform (DCT) (15), or multigrid methods (16). When some reliable predetermined quality map is available, the error function can be weighted pixel-by-pixel by the quality map to reduce the effects of background noise and unreliable pixels. The weighted least-squares problem is usually solved by iterating the unweighted method (17), and hence, it is slower than the unweighted counterpart. Performance of these methods is also heavily dependent on the quality of the weighting matrix. A generalized L^p-norm method (8) has been proposed to use data-dependent weights, which iteratively solves for unwrapped phased and updates the weights. This method has proven to be effective, but it is computationally demanding. Some least-squares methods also involve the use of an explicit phase model, for example, a polynomial model (18). To satisfy the congruent test, the model error (assumed to be in the principal value range) is added back to the final solution (18).

The branch-cut algorithms restrict the integration through the image to paths without discontinuities (7). Specifically, these algorithms assume that phase discontinuities lie on the paths between the positive and the negative residues, known as branch cuts. A unique, self-consistent unwrapped phase function can result by selecting an integration path that avoids these discontinuities. Several algorithms have been proposed to search the phase image only once for the optimal branch cuts. De-

pending on definition for optimality, some attempt to minimize the sum of the cut lengths (19), or to take advantage of the information from the particular application (9), and other algorithms use a quality map to assist selection of branch cuts based on region growing methods (20). Hybrid algorithms combining both the branch-cut and the region growing methods have also been proposed with some success (21).

Similar to the branch-cut methods, the network flow methods (22,23) are based on the same assumption that phase discontinuities lie on the paths between the positive and the negative residues. The difference is that instead of avoiding these discontinuities, the network flow methods explicitly quantify the discontinuities pixel by pixel and then minimize the overall discontinuities in the unwrapped phase image. Additional information such as a quality map can also be incorporated into the algorithm (24). Minimum and maximum spanning tree methods have been used to simplify the network flow (25–27), which leads to computationally efficient methods (28). More recent phase unwrapping methods in this category employ statistical costs for minimizing the discontinuities (29–32).

2.2. State-of-the-Art Algorithms

This section provides a summary of the algorithmic details of several state-of-the-art algorithms and a brief discussion of their strengths and limitations.

2.2.1. Least-Squares Methods.

2.2.1.1. Procedure. The least-squares methods find the unwrapped phase that minimizes the following cost in a least-squares sense:

$$J = ||\Delta\phi^x - \mathcal{W}(\Delta\psi^x)|| + ||\Delta\phi^y - \mathcal{W}(\Delta\psi^y)||. \tag{11}$$

To achieve the minimization, the FFT-based unweighted least-squares method first extends the wrapped phase to a periodic function $\tilde{\psi}$ by performing a mirror reflection about the last row and the last column of the image. The unwrapped counterpart $\tilde{\phi}$ of the periodic extension is then obtained by solving the discrete form of a Poisson's equation, whose solution can be efficiently found through the 2-D inverse FFT of

$$\frac{P_{m,n}}{2\cos(\pi m/M) + 2\cos(\pi n/N) - 4}, \tag{12}$$

where $P_{m,n}$ is the 2-D FFT of $\tilde{\rho}_{m,n}$, which is defined as

$$\begin{aligned}\tilde{\rho}_{m,n} = &(\mathcal{W}(\Delta\tilde{\psi}^x_{m,n}) - \mathcal{W}(\Delta\tilde{\psi}^x_{m-1,n})) \\ &+ (\mathcal{W}(\Delta\tilde{\psi}^y_{m,n}) - \mathcal{W}(\Delta\tilde{\psi}^y_{m,n})).\end{aligned} \tag{13}$$

Finally, the unwrapped phase is given by restricting the obtained $\tilde{\phi}$ to the original image size.

2.2.1.2. Strengths and Limitations. The unweighted least-squares method is very fast because of the use of FFT, which in turn requires the dimensions of the wrapped phase image to be powers of two. However, the solution can be sensitive to the presence of residues, and the corruption can spread throughout the image. In addition, the resulting solution fails the congruent test and typically represents a smoother solution than what the data can conceivably support. Therefore, the least-squares algorithm is generally not suitable in applications with sharp features unless a reliable quality map can be obtained and incorporated into a weighted version of the algorithm; in which case, the computational complexity has to be compromised.

2.2.2. Branch-Cut Methods.

2.2.2.1. Procedure. In the branch-cut methods, we search for residues and balance them in a region by connecting opposite polarities with branch cuts. Thus, ambiguous unwrapping is avoided if, and only if, the integration occurs along any path that does not cross branch cuts. It is nontrivial to choose good branch cuts from the many ways to balance polarities. Wrapped phase values cannot prefer any set of branch cuts without ancillary information. In addition to balanced residues, some criteria must be established to guide the placement of branch cuts. A common criterion is to connect residues in such a way that minimizes the net length of branches. To achieve this minimization, the method constructs sets of locally connected and balanced branch cuts. Specifically, it begins with finding an unvisited residue and connecting to its nearest residue neighbor, regardless of polarity, using a branch cut. If the neighbor has not been visited previously, its polarity is added to the net sum for the current local branch-cut set. Otherwise, it is marked as visited to avoid its polarity being counted multiple times. The visit of neighbors continues until the net sum is neutral, or it reaches the image border; in which case, a branch cut is placed to the border. The residues in the local neighborhood are then designated balanced by the branch cuts. The algorithm then searches for another unvisited residue and constructs a new set of branch cuts until the entire image is visited. Refinements of this algorithm have included using a quality map to guide the search strategy, in which the visit starts from the high-quality pixels.

2.2.2.2. Strengths and Limitations. The branch-cut methods visit every pixel only once, and thereby they are extremely fast and require little memory. The computational time is close to that of the unweighted least-squares methods. And in many cases, the methods provide a robust and efficient unwrapping solution for images with low phase noise. However, the solution can be spatially incomplete in regions with large noise because the optimization in the branch-cut methods is performed on a local rather than on a global basis.

2.2.3. Network Flow Method.

2.2.3.1. Procedure. In this method, the phase unwrapping problem is regarded as minimization of the cost of a network flow. To construct a network, each local closed path used to evaluate the residues is defined as a node in the network. The nodes are connected by directed arcs whose direction is determined by the polarity of the res-

idues. The pixels lie between the network arcs and the nodes. Associated with each arc is a flow that moves from nodes with positive residues to those with negative ones. The flow in phase unwrapping corresponds to the integer multiples of 2π to be added to the wrapped phase gradient. The unwrapping problem looks for an optimal flow in each arc that minimizes the sum of costs for all arc flows, in which the cost per unit flow assigned to each arc is a critical design parameter in the optimization process and is kept low in general at the place of a real discontinuity or noisy regions. With the optimal flow, calculating the unwrapped phase is to sum along any paths the phase gradient, which is adjusted if there is a flow in the arc crossing the path of integration.

2.2.3.2. Strengths and Limitations. Because the network flow method searches for a global optimal solution, it permits robust phase unwrapping in many cases of isolated areas of low noise, even without use of a quality map. If a reliable quality map is available, it can be easily incorporated into the algorithm by assigning a spatially dependent cost per unit flow. Despite these advantages, the use of this method is limited by its intensive memory usage and its large computational complexity, which is also image dependent.

2.2.4. Simulations. A synthetic dataset was used to study the robustness of each algorithm to undersampling and noise, where the original true phase is assumed to be a 2-D Gaussian but truncated with a steep slope plane, as shown in Fig. 7, and its wrapped phase satisfies Equation 8 and therefore can be unwrapped perfectly.

2.2.4.1. Undersampling. When. the wrapped phase image is undersampled, as shown in Fig. 8a, the gradient of the slope plane becomes greater than π, which causes the path-dependent problem. To demonstrate the performance of the algorithms described in this section, we apply the unweighted least-squares, Goldstein's branch-cut, and Flynn's minimum discontinuity algorithms as representatives in each category to unwrap the phase, and the unwrapping results are shown in Fig. 8b–d, respectively. The results show that both the least-squares method and the branch-cut method fail to unwrap the phase correctly at the location of undersampling. Compared with the least-squares method, the error of the branch-cut method is more localized and is a multiple of 2π. In contrast, the Flynn algorithm can unwrap the phase exactly.

2.2.4.2. Noise. When additive noise is present, the wrapped phase becomes $\mathcal{W}(\Phi + n)$, where n is the additive white Gaussian noise. The noisy wrapped phase of Fig. 7 is shown in Fig. 9a. As noise increases, the total number of residues increases, which results in high deviation of the unwrapped phase from the true phase.

Figure 9b–d show the unwrapped results of the unweighted least-squares, Goldstein's branch-cut, and Flynn's minimum discontinuity algorithms. In the presence of large noise, the least-squares approach fails completely because it cannot detect the edges of the interferogram from the smoothing effects, and the branch-cut method results in block errors because the residues become difficult to balance. Compared with these two methods, Flynn's algorithm gives the best results.

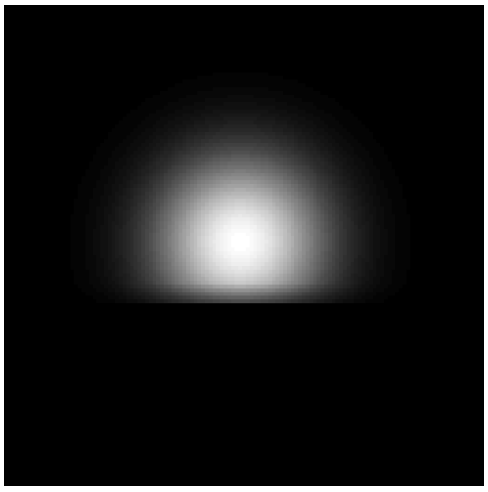

Figure 7. A synthetic dataset used as the original true phase to test the performance of different algorithms.

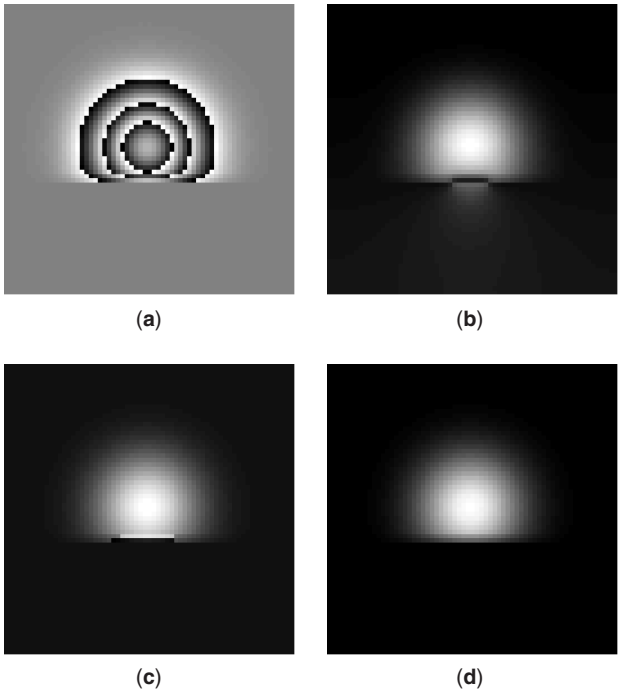

Figure 8. When the wrapped phase image in (a) is undersampled, the phases unwrapped by the (b) least-squares and the (c) branch-cut method have artifacts at sharp edges. The (d) Flynn method is observed to perform well.

3. APPLICATIONS IN MAGNETIC RESONANCE IMAGING

Among many applications of phase unwrapping, this article only focuses on the applications in MRI. In most clinical study, MRI is only limited to providing magnitude

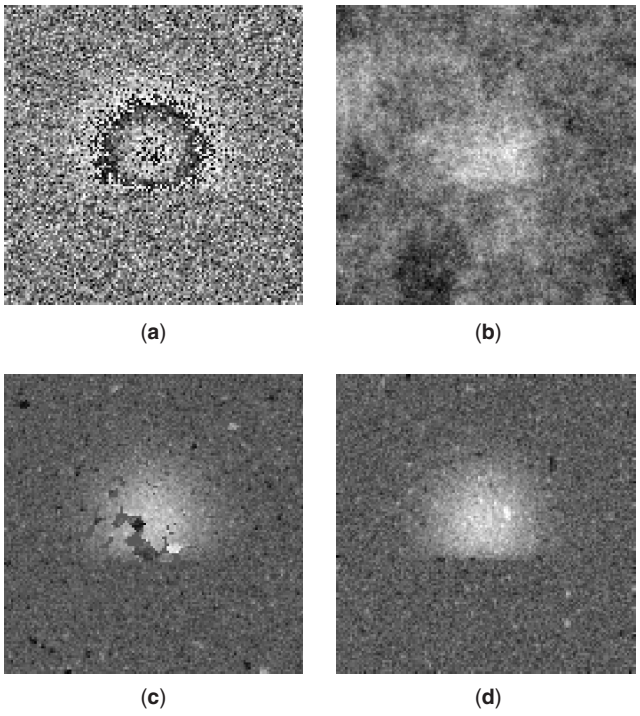

Figure 9. Because of noise in the complex signal, the obtained (a) wrapped phase is difficult to unwrap. Comparison of unwrapping results using the (b) least-squares, the (c) branch-cut, and the (d) Flynn's methods shows that the Flynn's method is more robust.

images. In fact, the phase of MR images also carries rich information about field inhomogeneity, velocity of blood flow, temperature variations, chemical shifts, and so on.

3.1. Field Inhomogeneity Mapping

The field inhomogeneity is an important cause of distortion in MRI. If it cannot be kept low enough, the inhomogeneity should be measured so that some form of correction scheme can be applied.

The field inhomogeneity map is obtained from the phase information of the image reconstructed using the echo time encoding technique. Specifically,

$$E(x, y) = -\frac{\phi_{x,y}}{\gamma \Delta_t}, \tag{14}$$

where field inhomogeneity term $E(x, y)$ denotes the field difference from B_0 at point (x, y), $\phi_{x,y}$ is the phase of the complex image, and Δ_t is the time interval between the radio-frequency (RF) echo center and the gradient echo center. It is observed that by choosing appropriate Δ_t, the field inhomogeneity is obtained from the phase so that the distortion can then be corrected. However, if Δ_t is chosen such that the phase $\phi_{x,y}$ is not always within one cycle of 2π, phase unwrapping is necessary because only $\psi_{x,y}$ can be directly obtained from the argument of the complex image $\hat{\mathbf{I}}(\hat{x}, \hat{y})$.

Field inhomogeneity can be caused by several factors. Static B_0 field inhomogeneity is present in most MRI systems. Other important causes include chemical shift and susceptibility effects. The B_0 field inhomogeneity is usually small within the imaging region and is slowly varying in space; therefore, most phase unwrapping algorithms can handle this type of field inhomogeneity. On the other hand, the susceptibility effects cause the field to change rapidly in space, which results in complications in phase unwrapping. Figure 10 presents a challenging unwrapping example, where Fig. 10a shows the phase of an MRI head image using a gradient-echo sequence at 1.5 T. It is seen that the air–tissue interface (e.g., the nasal and oral cavity areas) is difficult to unwrap because of the susceptibility effects. Figure 10b shows the unwrapped phase using the least-squares method. The method generates a smooth field map, but it may not correctly represent all field variations.

3.2. Phase-Sensitive Inversion Recovery

In MRI, inversion recovery imaging is one of the most useful techniques to improve image contrast. Instead of the conventional magnitude image, inversion recovery often requires display of the real part of a complex image because the contrast enhanced image often contains negative values. However, in practice, phase errors from filed inhomogeneity and data sampling window offset usually need to be corrected before the display to avoid loss of contrast and polarity artifacts (33). Phase unwrapping techniques can be used to estimate and thereby correct the phase errors. Figure 11a shows the inversion recovery image of a brain without phase correction, in which the intensity is slowly modulated by the phase errors. Figure 11b is the corresponding image after phase correction, in which the phase error is estimated using the least-squares method. The image improvement demonstrates the necessity of phase estimation and correction.

3.3. Flow Imaging

The first work for motion detection of seawater by nuclear magnetic resonance was done by Hahn (34), which was followed by its first MRI application (35). After additional work by Van Dijk (36) and Bryant et al. (37), phase-shift velocity mapping has become an important clinical tool for quantitative *in vivo* flow measurement in large vessels.

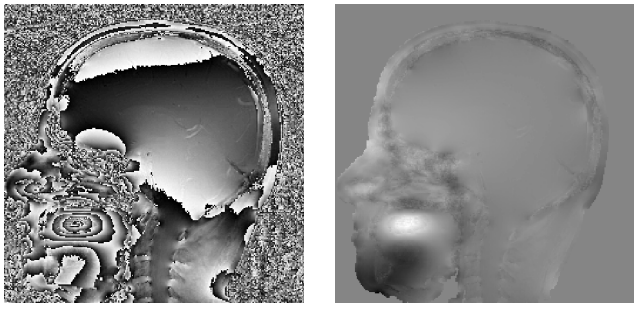

Figure 10. (a) Phase image of an MR head image and (b) the corresponding field map obtained using phase unwrapping.

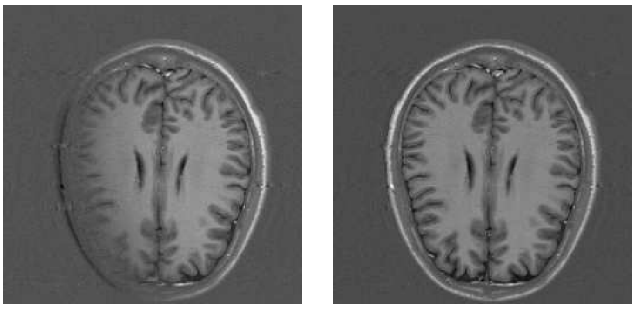

(a) (b)

Figure 11. Inversion recovery image (a) before and (b) after phase correction.

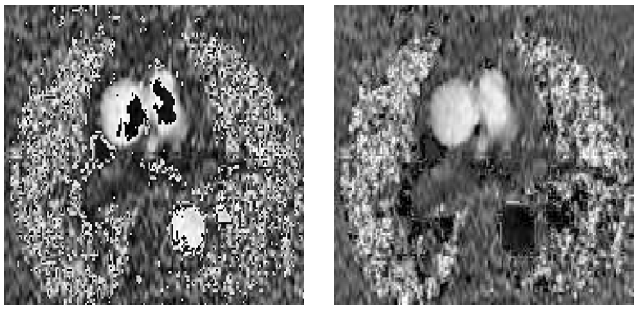

(a) (b)

Figure 12. In flow imaging, the (b) velocity map is obtained through unwrapping the phase in (a). The bright circles denote flow with positive direction, and the dark circle denotes a negative

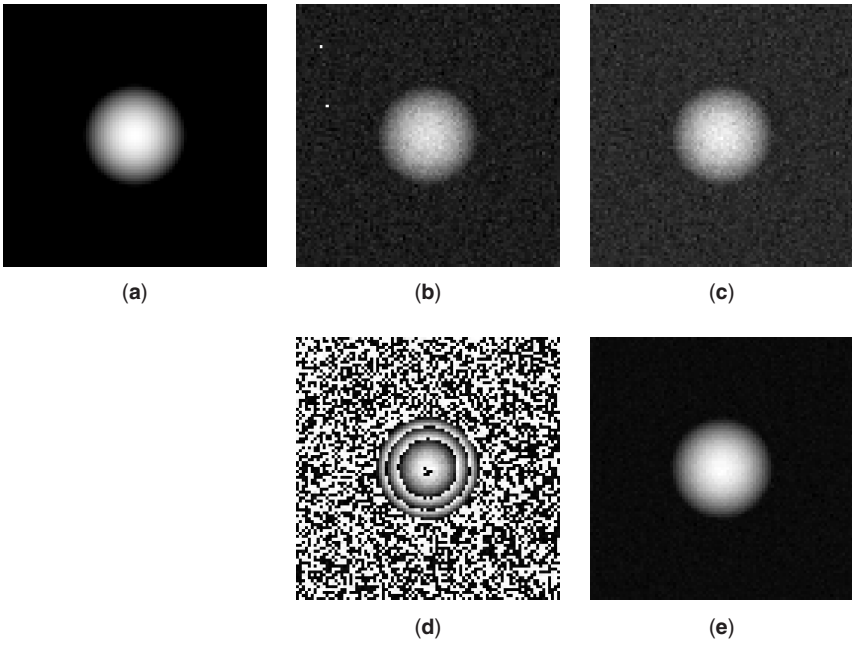

(a) (b) (c) (d) (e)

Figure 13. A (a) parabolic profile is used to simulate idealized laminar flows. When a large VENC is used to encode the velocity to the wrapped phase in (b), unwrapping is hardly needed to acquire the (c) velocity map. For a small VENC, there are closely spaced fringes in the (d) wrapped phase, which makes unwrapping more challenging. However, the resulting (e) velocity map has reduced noise.

The technique relies on the fact that the transverse magnetization of spins moving in the direction of a field gradient exhibits a motion-related phase shift. Specifically, if constant velocity motion is assumed, a phase shift is created by the transverse magnetization and is proportional to the scalar product of velocity v and the first moment of the time-varying gradient field $G(t)$; i.e.,

$$\hat{\mathbf{I}}(x,y) = \mathbf{I}(x,y)e^{j\gamma v(x,y)\cdot\int_0^T tG(t)dt}. \qquad (15)$$

The velocity of the moving spins along the direction of G can be inferred by

$$v(x,y) = \frac{\phi_{x,y}}{\gamma \int_0^T tG(t)dt}. \qquad (16)$$

Again, if the phase $\phi_{x,y}$ is not always within one cycle of 2π, phase unwrapping is necessary. Figures 12a and b show the phase map of a velocity-encoded image of blood vessels and the corresponding velocity map using Flynn's unwrapping method, in which the top two bright circles denote the blood flows toward the reader and the lower dark circle denotes the opposite. Theoretically, phase unwrapping can be avoided by properly choosing *G(t)* as described in the next section. However in practice, when the velocity distribution has substantial spatial or temporal variations, phase wrapping is unavoidable.

3.4. Effect of Imaging Parameters

Selection of imaging parameters is important to measure the field inhomogeneity or flow velocity accurately using phase. For example, in flow imaging, the gradient waveform *G(t)* is the imaging parameter to be chosen carefully. It can be neither too large because of the increased phase unwrapping challenge nor too small because of noise amplification. According to Equation 16, phase shifts $\phi_{x,y}$ do not need to unwrap if the maximum possible velocity is less than $(\pi/\gamma \int_0^T tG(t)dt)$, the so-called VENC. If the velocity values exceed this limit, phase wrapping occurs, AU:2

which means that to avoid phase unwrapping, a large VENC or a small *G(t)* is preferred. On the other hand, a large VENC amplifies the random noise and sacrifices velocity sensitivity, which is crucial in most clinical practices where the velocity is required to be quantified. Therefore, there is a tradeoff between high sensitivity (low noise) and phase unwrapping accuracy. Figure 13 illustrates this tradeoff in flow measurement. A parabolic profile is used to simulate idealized laminar flows, as shown in Fig. 13a. When a large VENC is applied, phase wrapping can be avoided, as shown in Fig. 13b, but the corresponding velocity map in Fig. 13c has large noise. With the same SNR in the complex MR signal, small VENC reduces noise in the velocity map as in Fig. 13e when the least-squares method is used, although the closely spaced phase fringes shown in Fig. 13d present difficulty in phase unwrapping. General knowledge about the velocity range in different parts of the cardiovascular system is usually used to determine a suitable *G(t)* and *T* for flow imaging. However, a correct velocity range is not always easily predictable, especially for patients with altered cardiovascular morphology or function (38), which makes powerful phase unwrapping algorithm indispensable.

4. CONCLUSIONS

The phase unwrapping is not a new topic; it has been studied for several decades. Interested readers should refer to Ref. 8 for detailed descriptions and source codes of various established algorithms. It is apparent that phase unwrapping is a difficult task. In practice, additional information is usually required to obtain the desired results. How to successfully incorporate additional information is still an open issue and is application-dependent. The researcher must have a thorough understanding of the physical problem underlying phase unwrapping. With the rapid development of MRI, the information in phase will be more highlighted and used. The future of phase unwrapping is promising but also challenging. With continued advancements, phase unwrapping will find more engineering applications and lead to new discoveries.

BIBLIOGRAPHY

1. C. V. Jakowatz, Jr., D. E. Wahl, P. H. Eichel, D. C. Ghiglia, and P. A. Thompson, *Spotlight Mode Synthetic Aperture Radar: A Signal Processing Approach*. Boston: Kluwer Academic Publishers, 1996.
2. G. H. Glover and E. Schneider, Three-point dixon technique for true water/fat decomposition with inhomogeneity correction. *Magn. Reson. Med*. 1991; **18**:371–383.
3. D. L. Fried, Least-squares fitting a wave-front distortion estimate to an array of phase-difference measurements. *J. Opt. Soc. Amer. A*. 1997; **67**(3):370–375.
4. K. Itoh, Analysis of the phase unwrapping problem. *Appl. Opt*. 1982; **21**(14):2470.
5. D. C. Ghiglia, G. A. Mastin, and L. A. Romero, Cellular automata method for phase unwrapping. *J. Opt. Soc. Amer. A*. 1987; **4**(1):267–280.
6. E. Kreysig, *Advanced Engineering Mathematics*. New York: Wiley, 1966.
7. R. M. Goldstein, H. A. Zebker, and C. L. Werner, Satellite radar interferometry: two-dimensional phase unwrapping. *Radio Sci*. 1988; **23**:713–720.
8. D. C. Ghiglia and M. D. Pritt, *Two-Dimensional Phase Unwrapping*: *Theory*, *Algorithms*, *and Software*. New York: Wiley, 1998.
9. S. Chavez, Q. S. Xiang, and A. Li, Understanding phase maps in MRI: a new cutline phase unwrapping method. *IEEE Trans. Med. Imag*. 2002; **21**(8):966–977.
10. J. M. Huntley, Three-dimensional noise-immune phase unwrapping algorithm. *Appl. Opt*. 2001; **40**:3901–3908.
11. M. Jenkinson, Fast, automated, N-dimensional phase unwrapping algorithm. *Magn. Reson. Med*. 2003; **49**:193–197.
12. W. B. Davenport, Jr. and W. L. Root, *An Introduction to the Theory of Random Signals and Noise*. New York: McGraw-Hill, 1958.
13. Q. S. Xiang, Temporal phase unwrapping for cine velocity imaging. *J. Magn. Reson. Imag*. 1995; **5**:529–534.
14. M. D. Pritt and J. S. Shipman, Least-squares two-dimensional phase unwrapping using FFTs. *IEEE Trans. Geosci. Remote Sensing* 1994; **32**(3):706–708.
15. D. Kerr, G. H. Kaufmann, and G. E. Galizzi, Unwrapping of interferometric phase-fringe maps by the discrete cosine transform. *Appl. Opt*. 1996; **35**(5):810–816.
16. M. D. Pritt, Phase unwrapping by means of multigrid techniques for interferometric SAR. *IEEE Trans. Geosci. Remote Sensing* 1996; **34**(3):728–738.
17. S. M. Song, S. Napel, N. J. Pelc, and G. H. Glover, Phase unwrapping of MR phase images using Poisson equation. *IEEE Trans. Image Processing* 1995; **4**(5):667–676.
18. Z.-P. Liang, A model-based method for phase unwrapping. *IEEE Trans. Med. Imag*. 1996; **15**:893–897.
19. J. M. Huntley, Noise-immune phase unwrapping. *Appl. Opt*. 1989; **28**(15):3268–3270.
20. D. J. Bone, Fourier fringe analysis: the two-dimensional phase unwrapping problem. *Appl. Opt*. 1991; **30**(25):3627–3632.
21. C. Prati, M. Giani, and N. Leuratti, SAR interferometry: A 2-D phase unwrapping technique based on phase and absolute values information. *Proc. IGARSS* 1990: 2043–2046.
22. M. Costantini, A novel phase unwrapping method based on network programming. *IEEE Trans. Geosci. Remote Sensing* 1998; **36**(3):813–821.
23. T. J. Flynn, Two-dimensional phase unwrapping with minimum weighted discontinuity. *J. Opt. Soc. Amer A*. 1997; **14**(10):2692–2701.
24. C. W. Chen and H. A. Zebker, Network approaches to two-dimensional phase unwrapping: intractability and two new algorithms. *J. Opt. Soc. Amer. A*. 2000; **17**(3):401–414.
25. D. P. Towers, T. R. Judge, and P. J. Bryanston-Cross, Automatic interferogram analysis techniques applied to quasiheterodyne holography and ESPI. *Opt. Laser Eng*. 1991; **14**:239–281.
26. N. H. Ching, D. Rosenfeld, and M. Braun, Two dimensional phase unwrapping using a minimum spanning tree algorithm. *IEEE Trans. Image Processing* 1992; **1**:355–365.
27. M. Takeda and T. Abe, Phase unwrapping by a maximum cross-amplitude spanning tree algorithm: a comparison study. *IEEE Trans. Image Processing* 1992; **1**:355–365.

28. L. An, Q. S. Xiang, and S. Chavez, A fast implementation of the minimum spanning tree method for phase unwrapping. *IEEE Trans. Med. Imaging* 2000; **19**(8):805–808.
29. J. M. B. Dias and J. M. N. Leitao, A discrete/continuous minimization method in inter-ferometric image processing. *Proc. EMMCVPR* 2001: 375–390.
30. C. W. Chen and H. A. Zebker, Two-dimensional phase unwrapping with use of statistical models for cost functions in nolinear optimization. *J. Opt. Soc. Amer. A*. 2001; **18**(2):338–351.
31. R. Koetter, B. J. Frey, N. Petrovic, and D. C. Munson, Jr., Unwrapping phase images by propagating probabilities across graphs. *Proc. IEEE ICASSP* 2001: 1845–1848.
32. L. Ying, B. Frey, R. Koetter, and D. C. Munson, Jr., An iterative dynamic programming approach to 2-d phase unwrapping. *Proc. IEEE Int. Geosci. Remote Sensing Symp*. 2002: 469–471.
33. Q. S. Xiang, Inversion recovery image reconstruction with multiseed region-growing spin reversal. *J. Magn. Reson. Imag*. 1996; **6**:775–782.
34. E. L. Hahn, Detection of sea-water motion by nuclear precession. *J. Geophys. Res*. 1960; **65**:776–777.
35. P. R. Moran, A flow velocity zeugmatographic interlace for nmr imaging in humans. *Magn. Reson. Imag*. 1982; **1**:197–203.
36. P. Van Dijk, Direct cardiac NMR imaging of heart wall and blood flow velocity. *J. Comput. Assist. Tomogr*. 1984; **8**:429–436.
37. D. J. Bryant, J. A. Payne, D. N. Firmin, and D. B. Longmore, Measurement of flow with NMR imaging using a gradient pulse and phase difference technique. *J. Comput. Assist. Tomogr*. 1984; **8**:588–593.
38. G. Yang, P. Burger, P. J. Kilner, S. P. Karwatowski, and D. N. Firmin, Dynamic range extension of cine velocity measurements using motion-registered spatiotemporal phase unwrapping. *J. Magn. Reson. Imag*. 1996; **6**:495–502.

KEYWORDS

phase unwrapping, magnetic resonance imaging, field inhomogeneity, flow imaging

ABSTRACT

Phase unwrapping is the reconstruction of the original true phase of a wave from its modulo 2π values. It originates in a variety of applications, such as synthetic aperture radar, magnetic resonance imaging, and adaptive optics. In this article, the problem of two-dimensional phase unwrapping is defined and the challenges are addressed. A variety of established approaches to the problems are reviewed and compared, and their advantages and disadvantages are discussed. Among the many phase unwrapping applications, the article focussed on magnetic resonance imaging and explains how phase unwrapping is used in field mapping, inversion recovery, and flow imaging.